Chemostratigraphic and U–Pb geochronologic constraints on carbon cycling across the Silurian–Devonian boundary

Jon M. Husson [a,b,∗], Blair Schoene [b], Sarah Bluher [b], Adam C. Maloof [b]

[a] *Department of Geoscience, University of Wisconsin–Madison, 1215 W. Dayton Street, Madison, WI 53706, USA*
[b] *Department of Geosciences, Princeton University, Guyot Hall, Washington Road, Princeton, NJ 08544, USA*

A B S T R A C T

The Devonian Period hosts extraordinary changes to Earth's biosphere. Land plants began their rise to prominence, with early vascular vegetation beginning its colonization of near-shore environments in the latest Silurian. Across the Silurian–Devonian (Pridoli–Lochkovian) transition, carbon isotope analyses of bulk marine carbonates ($\delta^{13}C_{carb}$) from Laurentian and Baltic successions reveal a positive $\delta^{13}C_{carb}$ shift. Known as the Klonk Event, values reach +5.8‰, making it one of the largest carbon isotope excursions in the Phanerozoic. Assigning rates and durations to these significant events requires a robust, precise Devonian time scale. Here we present 675 micritic matrix and 357 fossil-specific $\delta^{13}C_{carb}$ analyses from the lower Devonian Helderberg Group of New York and West Virginia that exhibit the very positive $\delta^{13}C_{carb}$ values observed in other Silurian–Devonian basins. This chemostratigraphic dataset is coupled with 66 ID-TIMS U–Pb dates on single zircons from six ash falls intercalated within Helderberg sediments, including dates on the stratigraphically lowest Devonian ashes yet developed. In this work, we (*a*) demonstrate that matrix and fossil-specific $\delta^{13}C_{carb}$ values track one another closely in the Helderberg Group, (*b*) estimate the Silurian–Devonian boundary age in New York to be 421.3 ± 1.2 Ma (2σ; including decay constant uncertainties), and (*c*) calculate the time required to evolve from baseline to peak $\delta^{13}C_{carb}$ values at the onset of the Klonk event to be 1.00 ± 0.25 Myr. Under these constraints, a steady-state perturbation to the global carbon cycle can explain the observed excursion with modern fluxes, as long as DIC concentration in the Devonian ocean remained below ~2× the modern value. Therefore, potential drivers, such as enhanced burial of organic carbon, need not rely on anomalously high total fluxes of carbon to explain the Klonk Event.

© 2015 Elsevier B.V. All rights reserved.

1. Introduction

The Early and Middle Devonian (419.2–358.9 Ma; Becker et al., 2012) mark an acme in genus-level diversity of marine invertebrates (Alroy et al., 2008) and widespread tectonism associated with the initial closing of the Rheic ocean that separated the Laurussian and Gondwanan paleocontinents (Nance et al., 2010). The end-Silurian records the initial colonization of terrestrial ecosystems by vascular plants, and this process continued in the Early Devonian with the development of larger body sizes, seeds and leaves (Gensel, 2008). Macroscale root systems become prevalent in alluvial systems in the Lochkovian Stage (Raven and Edwards, 2001), broadly coeval with the initiation of a putative, 100-Myr

decline in atmospheric CO_2 that some attribute to the rise of a terrestrial biosphere (Berner and Kothavala, 2001).

At the dawn of this major biotic innovation in the global carbon cycle, basins that span the Silurian–Devonian transition record a large, positive excursion in the $\delta^{13}C$ values of carbonate rock ($\delta^{13}C_{carb}$). Values rise from 0 to +5.8‰ in Laurentian (Nevada, Oklahoma and West Virginia; Saltzman, 2002) and Baltic (Czech Republic and Carnic Alps; Buggisch and Mann, 2004) sections (Fig. 1), making the Silurian–Devonian boundary excursion one of the largest in the Phanerozoic Eon (Saltzman and Young, 2005). Known as the 'Klonk Event' after the location of the GSSP for the Silurian–Devonian boundary in the Czech Republic, the similar shape and magnitude of the excursions recorded in globally disparate basins, constrained biostratigraphically to be Silurian–Devonian in age, has led many to argue that it represents a perturbation to the global carbon cycle, with rising values in $\delta^{13}C_{carb}$ representing the evolving isotopic composition of global dissolved inorganic carbon ($\delta^{13}C_{DIC}$). Workers have invoked global regression and the weathering of exposed, isotopically heavy Silurian

∗ Corresponding author at: Department of Geoscience, University of Wisconsin–Madison, 1215 W. Dayton Street, Madison, WI 53706, USA. Tel.: +1 608 262 8960; fax: +1 608 262 0693.
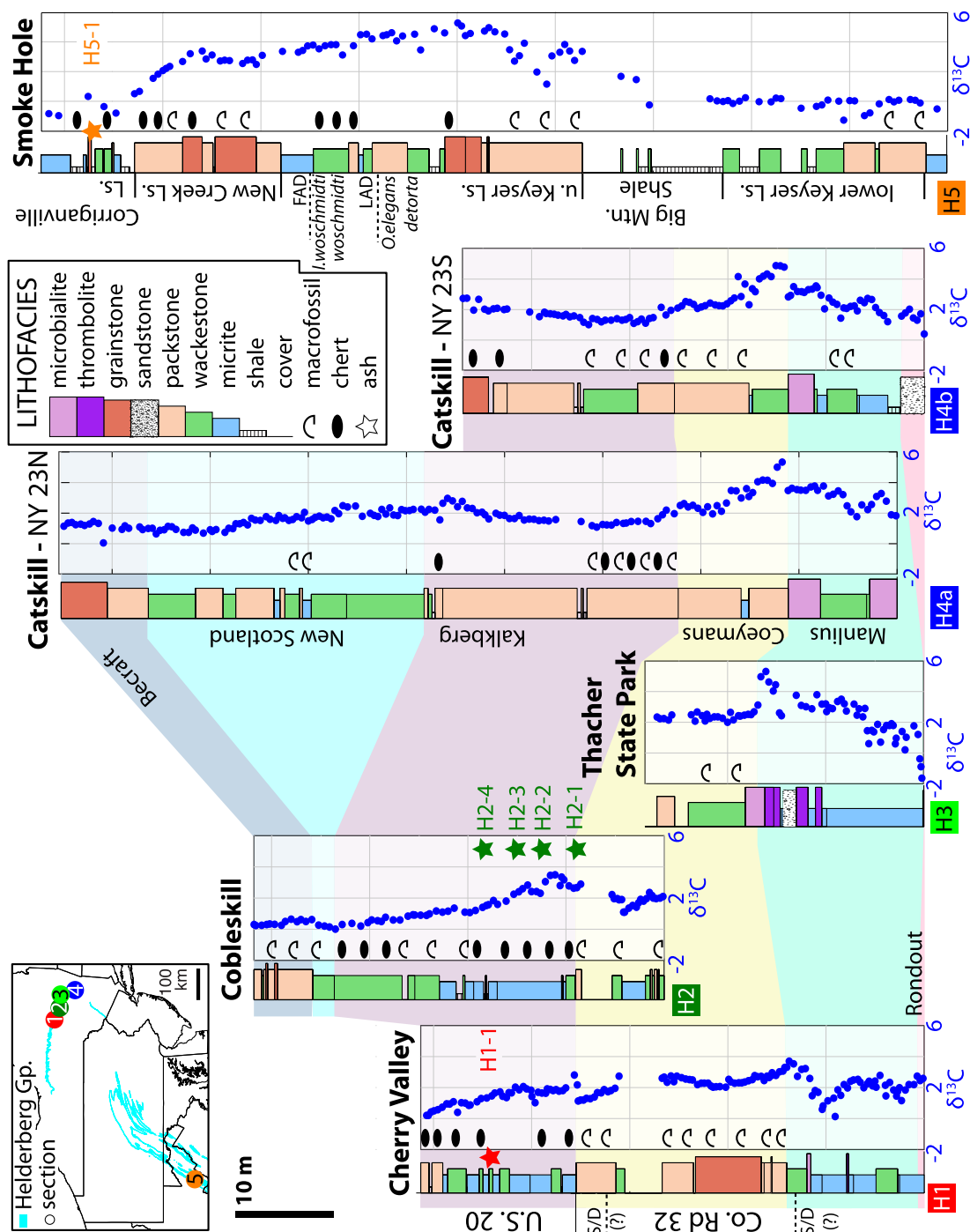*E-mail address:* husson@wisc.edu (J.M. Husson).

Fig. 1. (A) Silurian–Devonian $\delta^{13}C_{carb}$ data from the Czech Republic and the Carnic Alps (Buggisch and Mann, 2004), Oklahoma (Saltzman, 2002), Nevada (Saltzman, 2002), New York and West Virginia (sections H4 and H5 from this work). The similar shapes of the individual $\delta^{13}C_{carb}$ profiles have been used to create this composite, as well as biostratigraphic considerations for correlation at the epoch/age level. Despite divergences in $\delta^{13}C_{carb}$ values between localities, especially in the middle Lochkovian, all sections exhibit a positive $\delta^{13}C_{carb}$ excursion concordant with the Silurian–Devonian boundary. (B) The width of the bars, color-coded by section and lithology and labeled with true section thicknesses (in meters), correlates with $1/S$, where S is the stretch factor applied to the dataset; values of $1/S$ are labeled in the colored squares. If these stratigraphic $\delta^{13}C_{carb}$ profiles are a product of secular change in global DIC, then $1/S$ would also correlate with relative sedimentation rates of each section. (C) ~420 Ma paleogeographic reconstruction from http://www.gplates.org (Wright et al., 2013), with section localities rotated to their approximate paleo-position. (For interpretation of the references to color in this figure, the reader is referred to the web version of this article.)

carbonate platforms (Saltzman, 2002) or enhanced organic carbon burial of newly evolved terrestrial biota (Malkowski and Racki, 2009) as drivers for the Klonk Event. The general paradigm that (*a*) $\delta^{13}C_{carb}$ reflects $\delta^{13}C_{DIC}$ and (*b*) secular isotopic change is forced by changes to the global carbon cycle has been widely applied by geologists and geochemists to interpret global $\delta^{13}C_{carb}$ excursions (*e.g.*, Kump et al., 1999). Such models, however, rarely are coupled with independently-derived age models (Maloof et al., 2010), which would allow for intra- and inter-basin chemostratigraphic correlation schemes to be tested, the global vs. local nature of the $\delta^{13}C_{carb}$ excursion to be established, the absolute duration of the excursion to be constrained and the carbon fluxes and reservoir sizes required to drive the perturbation to be quantified. Therefore, a coupled chemostratigraphic-geochronologic study of the Silurian–Devonian boundary in the Helderberg Group of North America, where carbonate strata are interbedded with ash falls amenable to U–Pb dating on volcanic zircon, represents a rare opportunity to constrain rates of change and assess potential drivers for a major perturbation to the ancient geologic carbon cycle.

2. Geologic background

The Helderberg Group (Gp.) is a 90–140 m thick succession of mixed carbonates and siliciclastics (Clarke and Schuchert, 1899), deposited in a back-bulge Appalachian basin (*i.e.*, on the eastern margin of Laurentia, and west of the peripheral foreland bulge) in a period of relative tectonic quiescence between the Taconic and Acadian orogenies (Dorobek, 1987; Ver Straeten, 2004). It outcrops from central New York (measured sections H1–H4a,b on Fig. 2) to Virginia (H5 on Fig. 2), and is thickest near the axis of the Appalachian foreland basin in the Virginia–West Virginia region (Dorobek, 1987). Further north, the Heldeberg Gp. thins, and carbonate facies indicate a more restricted depositional environment, with basin isolation increasing from east to west in New York state (Rickard, 1962; Laporte, 1969). The Helderberg Gp. represents a transgressive system tract; in New York, deposition begins with the dolomite-cemented sandstones of the Rondout Formation (Fm.) which grades upward into the finely-bedded lagoonal carbonate mudstones with frequent microbialitic textures of the Manlius Fm. (Fig. 2). The more open-marine brachiopod–crinoid packstones and

Fig. 2. Physical stratigraphy of the Helderberg Gp., paired with $\delta^{13}C_{carb}$ data, from six measured stratigraphic sections. **Datum definitions:** The datum for sections H1, H3 and H4b is the base of the Rondout Fm. H2 begins in the Coeymans Fm., 9 meters below the Coeymans–Kalkberg contact. H4a begins in the Manlius Fm., 11 m below the Manlius–Coeymans contact. H5 begins in the Tonoloway. Limestone, 1.1 m below the Tonoloway Limestone–lower Keyser Limestone contact. Detailed locations for each measured section are outlined in section S1 of the supplementary online material.

grainstones of the Coeymans Fm. overlies the Manlius. The Coeymans fines upward into the cherty lime wackestones of the Kalkberg Fm., with a gradational contact existing with the overlying, finer argillaceous wackestones and mudstones of the New Scotland Fm. The overall fining-upward trend is interrupted briefly with the deposition of the thick-bedded, crinoidal grainstones of the Becraft Fm.

In West Virginia, the Keyser Limestone represents the lowest formation in the Helderberg Gp., and conformably overlies the

fossil-poor mudstones of the Tonoloway Limestone (Fig. 2). The wackestones and packstones of the Keyser Limestone are divided into upper and lower members by the ∼15-m-thick Big Mountain Shale. The upper Keyser Limestone grades into the coarser-grained packstones and grainstones of the New Creek Limestone, which in turn is overlain by the siltier, partially silicified mudstones of the Corriganville Limestone. Silicification increases upwards, and the Corriganville grades into the overlying Shriver Chert. Helderberg Gp. deposition ended with the Middle Devonian approach of the

Avalonian terrane towards the modern-day eastern side of Laurentia, which shed a vast quantity of siliciclastic material and buried the Helderberg Gp. in the Devonian–Mississippian Acadian clastic wedge (Dorobek, 1987).

The basal Devonian GSSP is located in Klonk, southwest of Prague, in the Czech Republic. The Klonk section is composed of rhythmically laminated limestones and shales, and the GSSP is within Bed 20, immediately below the first appearance of the graptolite *Monograptus uniformis uniformis* (Becker et al., 2012). Owing to its shallower, more carbonate-rich and coarser-grained nature, attempts at locating the Silurian–Devonian boundary in the Helderberg Gp. mainly have employed conodont biostratigraphy. In these efforts, identification of the first appearance datum (FAD) of the fossil sub-species *Icriodus woschmidti woschmidti* most commonly is used as a proxy for the base of the Devonian System (but see Carls et al., 2007, for a recent discussion of problems surrounding the use of *I. woschmidti woschmidti* as a basal Devonian index fossil). In West Virginia, the boundary is further constrained by the last appearance of the Pridoli-aged conodont *Oulodus elegans detorta* (Denkler and Harris, 1988). These biostratigraphic horizons imply that the Silurian–Devonian boundary is within the uppermost five meters of the Keyser Limestone (section H5 in Fig. 2). In the more restricted, fossil-poor facies of upstate New York, however, placement of the boundary is more challenging, and remains a subject of debate, with workers placing it variably between the top of the Rondout Fm. to as high as the upper Coeymans Fm. (Kleffner et al., 2009, and references therein). On Fig. 2, two horizons are labeled in section H1 that are described as the best candidates for the Silurian–Devonian boundary by Kleffner et al. (2009), based upon both biostratigraphic and chemostratigraphic considerations.

Coincident with basin transgression, as the succession transitions from shallow, shelfal carbonates to deeper, shalier units, numerous 2–20 cm thick ashes are found in the Helderberg Gp. (Ver Straeten, 2004). The clay-rich beds (K-bentonites) contain pristine volcanic phenocrysts of apatite, feldspars, β-quartz and zircon, and analysis of melt inclusions within quartz grains indicate parent magmas of a high-silica, rhyolitic composition (Hanson, 1995). These ashes have been used for over 50 years as an intra-basin correlation tool (Rickard, 1962; Hanson, 1995; Ver Straeten, 2004); however, only a single ash (sample H1-1 in Fig. 2) has been previously targeted for radioisotopic dating via U–Pb in zircon (Tucker et al., 1998). The age from Tucker et al. (1998) – a weighted-mean $^{207}Pb/^{206}Pb$ age calculated from 9 multi-grain ID-TIMS analyses – represents the oldest dated horizon from Devonian sediments. The age was recalculated by Schmitz (2012) to be 415.58 ± 2.71 Ma using the revised U decay ratio of Schoene et al. (2006), and serves as an important anchor-point for estimation of the absolute age of the Silurian–Devonian boundary, currently defined as 419.2 ± 3.2 Ma (Becker et al., 2012).

3. Methods

3.1. $\delta^{13}C$ and $\delta^{18}O$ chemostratigraphy

Carbonates were sampled at ~0.3 to 0.5 m resolution while measuring six stratigraphic sections covering the Helderberg Gp. Clean limestones and dolostones with minimal siliciclastic components were targeted. A total of 675 samples were slabbed and polished perpendicular to bedding and 5 mg of powder were micro-drilled from individual laminations of the finest-grained groundmass (most often micrite) for isotopic analysis. 357 powders also were micro-drilled from individual fossil domains (brachiopods, gastropods, crinoids, and corals) from bioclast-rich samples for comparison with micrite samples from the same horizons. Isotopic analyses were performed at Princeton University, where all powders were placed in individual borosilicate reaction vessels

and heated to 110 °C to remove volatile contaminants and water. Samples were then reacted at 72 °C with 5 drops of H_3PO_4 in a GasBench II preparation device coupled directly to the inlet of a Thermo DeltaPlus continuous flow isotope ratio mass spectrometer. $\delta^{13}C$ and $\delta^{18}O$ data were acquired simultaneously, and precision and accuracy of data are monitored through analysis of 21 standards for every 59 measured unknowns. 11 of the standards were an international, primary standard (NBS-19) and 10 were an internal marble standard. All $\delta^{13}C$ and $\delta^{18}O$ values are presented as ‰ differences from the isotopic composition of the V-PDB international standard. Measured precision is maintained at 0.1‰ (1σ) for $\delta^{13}C$ and 0.2‰ (1σ) for $\delta^{18}O$. All $\delta^{13}C$ and $\delta^{18}O$ measurements are provided in Tables S5 and S6 in the supplementary online material.

3.2. U–Pb zircon geochronology

All geochronology samples were processed and analyzed at Princeton University. Zircon crystals separated from the six ash samples were mounted in epoxy resin and imaged by cathodoluminescence (CL) to help screen for potential inherited populations (Fig. S1), with crystals selected for dating plucked from these mounts. Selected crystals had weak-to-strong concentric CL zoning, suggestive of a volcanic source (Fig. S1). After screening, selected zircons were prepared using a modified version of the chemical abrasion technique of Mattinson (2005), described fully in section S2 of the supplementary online material. All analyses were made on single zircon grains via isotope dilution, using either the EARTHTIME $^{205}Pb–^{233}U–^{235}U$ (ET535) or the $^{202}Pb–^{205}Pb–^{233}U–^{235}U$ (ET2535) tracer solution (see Table S1 for spike compositions; Condon et al., 2015; McLean et al., 2015). Isotopic ratios were measured on an IsotopX Phoenix62 thermal ionization mass spectrometer. Data reduction, error propagation and plotting of U–Pb data in Fig. 3 was done using the `U–Pb_Redux` software package (Bowring et al., 2011), using the algorithms of McLean et al. (2011). A full U–Pb data table is included in Table S4 in the supplementary online material, with reported uncertainties at the 2σ level that include internal sources of uncertainty only. More details on the geochronology and mass spectrometry methods employed are outlined in section S2 in the supplementary online material.

3.3. Zircon TIMS-TEA geochemistry

The trace element compositions of the same zircons dated by ID-TIMS were characterized following the analytical protocol of Schoene et al. (2010b) at Princeton University. Trace element washes isolated chromatographically during U–Pb column chemistry were dried down in pre-cleaned 2.0 ml polypropylene vials and redissolved in 1.0 ml 1.5 N HF + 0.1 N HNO_3 with 1 ppb Ir. Measurements were performed on a Thermo Fisher Element 2 sector field-inductively coupled plasma-mass spectrometer (SF-ICP-MS) with a sample introduction system consisting of a CETAC Aridus II desolvation nebulizer + ASX-100 autosampler. Measured elements included Zr, Hf, Sc, Y, Nb, Ta, REEs, Pb, U, Th and Ir, with iridium monitored as an internal standard during mass spectrometry. The instrument was tuned in medium resolution mode with an optimal signal intensity of 0.5–2 Mcps for 1 ppb Ir. A matrix-matched, gravimetric external calibration solution was prepared with the relative abundance of targeted elements matched to levels observed in natural zircon (*e.g.,* Zr/Hf = 50). A dilution series was generated using this solution to cover the range of concentrations observed in unknowns (*e.g.,* [Zr] = 10^1–10^4 ppb solution), which was then used to generate a concentration-intensity calibration curve for each trace element at the beginning of the analytical
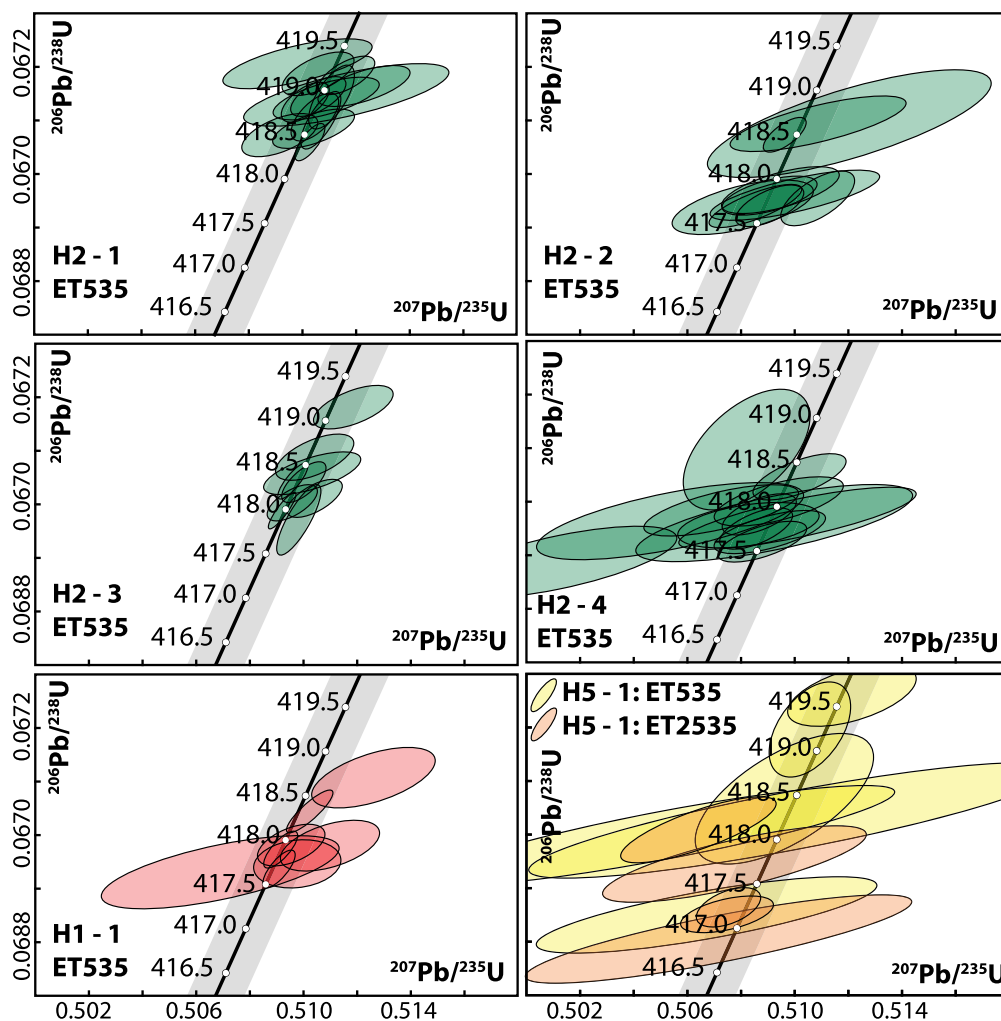
Fig. 3. Concordia plots for all dated zircons presented in this study. Labels beneath the sample names connote the EARTHTIME tracer used, either the ^{205}Pb–^{233}U–^{235}U (ET535) or the ^{202}Pb–^{205}Pb–^{233}U–^{235}U (ET2535) tracer (see Table S1). Error ellipses include analytical uncertainties only, are at the 95% confidence level and were calculated via the U-Pb_Redux program of Bowring et al. (2011) using the algorithms of McLean et al. (2011); U-Pb_Redux also generated the concordia plots.

session. Samples and interspersed instrumental and total procedural blanks were analyzed in sets of 24 with a line washtime of 120 s and uptake time of 90 s. Post data acquisition, solution concentrations were converted to stoichiometric concentrations in zircon by normalizing solution concentration data, assuming Zr + Hf = 497,646 ppm in zircon.

4. Results

4.1. Chemostratigraphy

We present 675 micritic matrix and 357 fossil-specific $\delta^{13}C_{carb}$ and $\delta^{18}O_{carb}$ analyses from six measured sections of the lower Devonian Helderberg Gp. in New York and West Virginia (Figs. 2 and 4). To account for differing thicknesses and sedimentation rates across the basin, heights of samples from individual sections were adjusted to create the composite Helderberg stratigraphic section presented in Fig. 4, with stretches designed to maximize the fit of their $\delta^{13}C_{carb}$ profiles, thereby assuming that $\delta^{13}C_{carb}$ change is isochronous at least on the basin-scale (unstretched stratigraphies are presented in Fig. 2). As H4 (a composite section of H4a and H4b; see Fig. 2 caption) is one of thickest and most stratigraphically complete sections presented here, it serves as reference against which the other 4 sections were stretched. By this design, H4 sample heights (in meters) correlate with their normalized po-

sition value (between 0 and 1; Fig. 4B) in the resulting composite on a 1:1 basis. Besides this reference section, individual sections need not have single stretch factors, nor is continuous sedimentation necessarily assumed. For example, data from H3 were treated as two blocks with different stretch factors, with a break between the upper and lower blocks (Fig. 4). This treatment implies a change in relative sedimentation rate in section H3 as compared to H4, with an inferred hiatus in deposition marking that change.

The basal portions of all measured sections show a distinctive rise in $\delta^{13}C_{carb}$ values, climbing from $\sim 0‰$ to $\sim 5‰$. In New York, this maximum occurs near the boundary of the Manlius and Coeymans fms., and is found in the basal upper Keyser Limestone in West Virginia (Figs. 2 and 4B). From this apogee, $\delta^{13}C_{carb}$ values fall to 1.5‰, and variably rise to a local maxima of 2 to 3‰ before falling to 1 to 2‰ at the top of the measured sections. $\delta^{13}C_{carb}$ data from fossil domains (red and blue bars in Fig. 4B), collected from bioclast-rich horizons in sections H1 and H4, closely track the $\delta^{13}C_{carb}$ values (*i.e.*, within $\sim 0.5‰$) developed from the coeval micrite phase. Such reproducibility is not apparent in the $\delta^{18}O_{carb}$ dataset, where fossils diverge from micrite by up to 4‰ and gradients of up to 7‰ exist between individual sections (Fig. 4B). The absence of stratigraphic coherence suggests a diagentic control on $\delta^{18}O_{carb}$.

To compare the measured isotopic ratios of fossil and groundmass micrite phases more quantitatively, we calculate a $\Delta^{13}C$ and
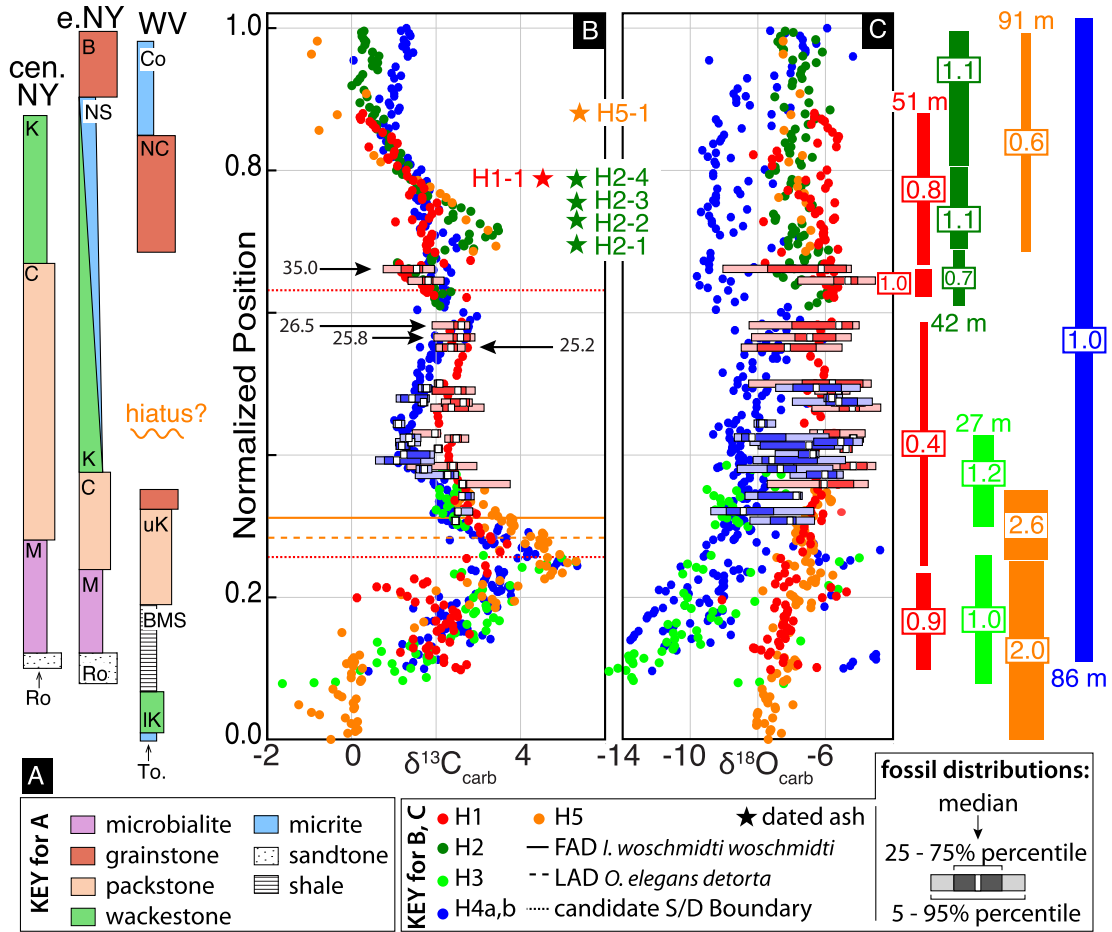
Fig. 4. (A) Lithostratigraphy of the Helderberg Gp., simplified from measured sections H1 (central New York), H4 (eastern New York; H4a and H4b are parallel sections, and are presented as this single composite section in this figure) and H5 (West Virginia). Composite $\delta^{13}C_{carb}$ (B) and $\delta^{18}O_{carb}$ (C) profiles for the Helderberg Gp., with individual sections stretched against H4 to maximize the fit in $\delta^{13}C_{carb}$. Other significant horizons, such as the FAD of *I. woschmidti woschmidti* and LAD of *O. elegans detorta* in West Virginia (Denkler and Harris, 1988), the candidate horizons in section H1 for the Silurian–Devonian boundary from Kleffner et al. (2009) and ash fall beds, have been stretched along with the $\delta^{13}C_{carb}$ data. Colored circles are data from fine-grained groundmass, whereas the colored bars are boxplot distributions of isotopic values measured from fossils (brachiopods, crinoids, gastropods and corals; *n* for each distribution ranges between 3 and 49, with a median value of 8). Fossil horizons labeled with numbers are presented also in Fig. 5. The different stretches (*S*) and translations applied to the five sections are displayed as colored bars to the right of (C), with the widths of bars correlating to 1/*S* and labeled with true section thicknesses in meters. Values of 1/*S* also are labeled in the colored squares. Formation abbreviations in (A) are Ro = Rondout; M = Manlius; C = Coeymans; K = Kalkberg; NS = New Scotland; B = Becraft; To = Tonoloway Limestone; K = Keyser Limestone; BMS = Big Mountain Shale; NC = New Creek Limestone; Co = Corriganville Limestone. (For interpretation of the references to color in this figure, the reader is referred to the web version of this article.)

$\Delta^{18}O$ value for each of the 357 fossil measurements from sections H1 and H4 (Fig. 5). While bioclasts are present throughout the Helderberg, especially in packstone and grainstone lithologies, our analyses were restricted to intervals where fossils large enough for micro-drilling were present. Unfortunately, these horizons do not include the intervals of greatest isotopic change (fossil symbols on Fig. 2). These metrics have been used in previous studies to compare isotopic offsets between fossils and ground-mass (*e.g.*, Samtleben et al., 2001; Batt et al., 2007; Brand et al., 2012), and are defined as the difference in carbon and oxygen composition between a fossil phase and the coeval micrite sampled from the same stratigraphic horizon (*i.e.*, $\Delta^{13}C = \delta^{13}C_{fossil} - \delta^{13}C_{micrite}$). Thus, values of 0‰ in Fig. 5 denote no isotopic difference between a fossil and paired micrite measurement. For H1, the $\Delta^{13}C$ mean on the full dataset is −0.10‰, with a standard deviation of 0.35‰ (Fig. 5A); for H4, the mean value is 0.05‰ (1σ = 0.25‰; Fig. 5B).

While the variance in the $\Delta^{13}C$ distribution is higher in H1 than in H4, both are centered near 0‰ and are broadly Gaussian in shape (Fig. 5A, B). By contrast, the shapes of the $\Delta^{18}O$ distributions are very dissimilar, both from each other and from their associated $\Delta^{13}C$ distribution. For H1, the mean is close to zero (−0.12‰), but the distribution is very non-normal, and skews towards negative

$\Delta^{18}O$ values (Fig. 5C). The H4 $\Delta^{18}O$ distribution is more symmetric, but its mean is centered over 1.5‰ (Fig. 5D). In both instances, $\Delta^{18}O$ values are more dispersed than $\Delta^{13}C$; the observed range for $\Delta^{18}O$ is ~5‰, as compared to ~1‰ for $\Delta^{13}C$.

Differences between H1 and H4 fossil data also are apparent in cross-plots of $\Delta^{13}C$ and $\Delta^{18}O$ (Fig. 5E, F). H4 fossils exhibit no correlation between the two parameters, with larger variance in $\Delta^{18}O$ (Fig. 5F), analogous to the full Helderberg $\delta^{13}C_{carb} - \delta^{18}O_{carb}$ chemostratigraphic dataset (Figs. 4B, C and S2). By contrast, H1 fossils do show a linear correlation between $\Delta^{13}C$ and $\Delta^{18}O$ ($r^2 = 0.34$ with $p \ll 0.01$; Fig. 5E). This covariation is driven entirely by data from four stratigraphic horizons (colored squares in Fig. 5E; also labeled in Fig. 4B). Considering data from these four horizons only, the r^2 value is higher than the full dataset (0.57; $p \ll 0.01$); if these samples are excluded, fossil data from the remaining 11 horizons are uncorrelated, with an r^2 value of 0.06.

4.2. Depositional ages from U–Pb geochronology

In order to quantify the rates of isotopic change observed in the Helderberg Gp., as well as test the correlation model for the five sections derived from $\delta^{13}C_{carb}$ profiles, 10 potential ashes found
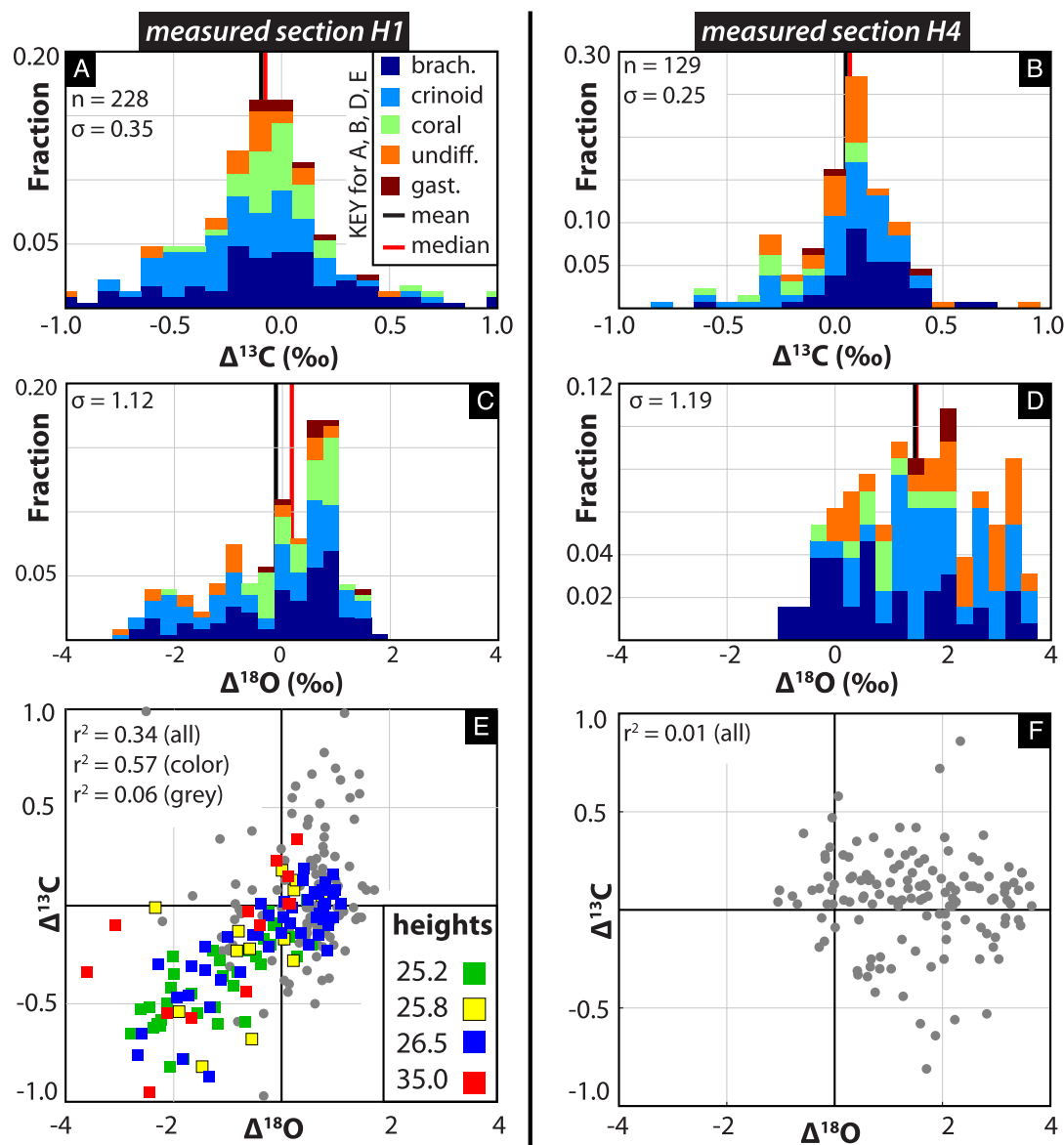
Fig. 5. Isotopic differences between fossil and micrite phases from measured sections H1 (15 horizons sampled) and H4 (16 horizons). $\Delta^{13}C$ is defined as $\delta^{13}C_{fossil} - \delta^{13}C_{micrite}$, whereas $\Delta^{18}O$ is an equivalent calculation for $\delta^{18}O$ values. These quantities are displayed as histograms (A–D) and as cross-plots (E, F). Legend values in (E) are stratigraphic heights (m) of samples plotted as colored squares and are relative to the H1 datum (Fig. 2).

throughout the Helderberg Gp. were sampled for U–Pb dating of zircon relative to EARTHTIME ($\pm^{202}Pb$)–^{205}Pb–^{233}U–^{235}U tracer solutions (Condon et al., 2015; McLean et al., 2015) by isotope-dilution thermal ionization mass spectrometry (ID-TIMS; see sections 3.2 and S2 for detailed geochronologic methods and Table S1 for spike compositions). Of these, six samples from three sections yielded prismatic, non-detrital zircon grains, and are interpreted as ash-fall horizons; cathodoluminescence (CL) images of select grains are shown in Fig. S1. In New York, all ashes were collected from the Kalkberg Fm. In section H2, four were collected, covering 9.4 m of stratigraphic distance with the most basal ash (H2-1) located on the Coeymans–Kalkberg boundary (Fig. 2). In section H1, one ash was collected ∼9 m above the Coeymans–Kalkberg boundary (Fig. 2). In the West Virginia section (H5; Fig. 2), one ash was collected from the Corriganville Limestone, 3.2 m above the New Creek–Corriganville boundary. In total, single-crystal radioisotopic dates on 66 euhedral zircons, ranging in long axis length from 50 to 500 μm, are presented here (Figs. S1, 3 and 6 and Table S4). The $^{206}Pb/^{238}U$ dates have been corrected for initial ^{230}Th disequi-

librium, using a Th/U ratio of the parent magma of 2.8 ± 0.5 (see section S2), and are displayed graphically as a rank-order plot in Fig. 6.

Single ash-fall samples show considerable dispersion in zircon dates, varying between 1 to 3 Myr (Fig. 6). Due to the analytical precision of individual analyses (0.05–0.075%, or ∼0.2–0.3 Myr), the ash spectra cannot be characterized as representing a single-aged population, and weighted-mean statistics, which would improve the precision for an assigned depositional age, are not appropriate. Interpretation of these complex date spectra is aided by trace element analysis on the analyzed zircon (TIMS-TEA data; Fig. 7). For example, a trend of decreasing [Nb] with increasing age (Fig. 7A), and possibly of decreasing Th/U with increasing age (Fig. 7D), within the H2 group of four ashes supports the claim that each horizon is a distinct ash fall event, recording long-term trends in the geochemical evolution of the volcanic system generating these ashes, and are not four instances of reworking of the same ash. While the date spectra cannot be characterized as representing a single-aged population, sub-populations of zircon within
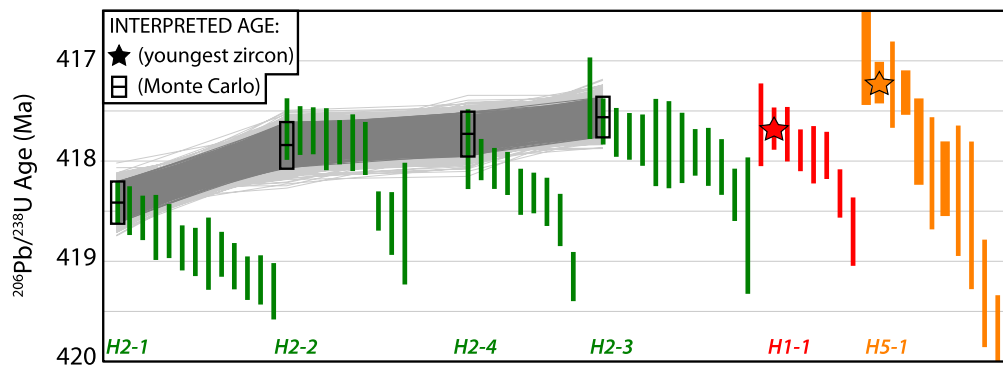
Fig. 6. $^{206}Pb/^{238}U$ dates on single zircon crystals from six ashes, color-coded to section locations presented in Figs. 2 and 4. Error bars describe analytical uncertainty only (2σ), with thinner bars corresponding to analyses using EARTHTIME $^{205}Pb-^{233}U-^{235}U$ tracer and thicker bars to analyses using the $^{202}Pb-^{205}Pb-^{233}U-^{235}U$ tracer (only the H5 sample includes $^{202}Pb-^{205}Pb-^{233}U-^{235}U$ analyses). Interpreted depositional ages for a given ash sample are marked either with a star or a black outline, the latter of which is the result of Monte Carlo re-sampling of the initial estimate of the eruption age (light grey lines show acceptable fits, with the darker grey region indicating the resulting age model; see section 4.3 for more details). Interpreted ages are also presented in Table 1. (For interpretation of the references to color in this figure, the reader is referred to the web version of this article.)

single ash samples can be identified that form groups overlapping in age, and might be amenable to weighted mean statistics. These sub-groups, however, show considerable diversity in their geochemistry. The most dramatic example can be found in H2-2 (green squares), in which 7 zircons comprise a well-defined age plateau (Fig. 6). These same zircon, however, cover a large range in [Nb], [Hf], [Y] and Th/U, thus suggesting that they are not a co-genetic population (Fig. 7). These observations suggest that populations of zircon in ash beds represent a diversity of processes occurring within the volcanic system – *e.g.*, prolonged zircon growth in the magma chamber or the incorporation of antecrystic or xenocrystic zircon from the volcanic edifice during eruption and transport – and encourage a cautious approach to the use of weighted mean statistics for this geochronologic dataset.

We therefore use the youngest closed system zircon as the most accurate and conservative approximation of the depositional age (see Table S2 for alternative age interpretations). For H2-1, H2-2 and H2-3, the youngest zircon in the population was selected; for H2-4, H1-1, and H5-1, the second-youngest was selected, due to reverse discordance (H2-4 and H1-1; Fig. 3) or relatively high Pb blank levels (H5-1-z22 in Table S4) observed in the youngest zircon analyses for these samples. Within the H2 ashes, all taken from the same stratigraphic section, the observation that the interpreted age either youngs upwards (namely, from H2-1 to H2-4) or overlaps in analytical uncertainty strengthens the case for use of the youngest zircon approach (Schoene et al., 2010a).

4.3. Monte Carlo approach to depositional ages

In cases where stratigraphic order is known, depositional age models can be refined further through Monte Carlo re-sampling of the initial age estimate (*e.g.*, Meyers et al., 2012; Guex et al., 2012). Within an undisturbed stratigraphic section, the law of superposition requires that depositional age youngs upward, and this requirement can be used to improve estimates of depositional ages of ash beds in the Helderberg Gp. This approach is especially helpful in cases where depositional ages overlap in uncertainty, as they do in H2-2, H2-3 and H2-4 (Fig. 6). The model produces 10^6 synthetic dates, drawn from a normal distribution defined by the initial estimate of the depositional age with its uncertainty, for each ash age interpretation. This approach is applied only to the H2 group, as all came from a single stratigraphic section, and thus the stratigraphic ordination of H2-1, H2-2, H2-3 and H2-4 is known with certainty. A path (*i.e.*, a set of four ages for each of the four ashes) is created by randomly selecting a point from each of the synthetic datasets. If the path is stratigraphically valid (*i.e.*, youngs

upwards), then the path is kept. A valid path results in a new age assignment for each ash layer. After a million path evaluations, the results are four new distributions that are broadly Gaussian; the mean and standard deviation of each new distribution is taken as the new best estimate for the age and uncertainty (2σ level) of the ash in question (dark, open outlines in Fig. 6A; Table 1).

5. Discussion

5.1. Isotopic offsets between fossil and micrite phases

In sections H1 and H4 (Figs. 2 and 4), bioclast-rich horizons were sampled for fossil-specific $\delta^{13}C_{carb}$ and $\delta^{18}O_{carb}$ (Fig. 4B, C), with offsets between fossil and micrite phases quantified as $\Delta^{13}C$ and $\Delta^{18}O$ values (Fig. 5). For carbon (Fig. 5A, B), fossil $\Delta^{13}C$ distributions are normal and centered near 0‰, with mean $\Delta^{13}C$ values independent of fossil type (*i.e.*, brachiopod, crinoid, gastropod, or coral; see Table S3). The fossil $\Delta^{13}C$ distributions also exhibit low variance, especially when compared to the large-scale $\delta^{13}C_{carb}$ signals recorded in Helderberg micrite (changes of 5–6‰; Fig. 4B). These observations suggest that the dominant factor controlling $\delta^{13}C_{carb}$ in different phases of Helderberg sediment is the $\delta^{13}C$ of the precipitating fluid.

Insights into processes leading to greater variability in H1 fossil $\Delta^{13}C$ can be found in its associated $\Delta^{18}O$ dataset (Fig. 5C). In H1, fossil $\Delta^{13}C-\Delta^{18}O$ values are correlated strongly (Fig. 5E), in marked contrast to the lack of covariation between fossil $\Delta^{13}C$ and $\Delta^{18}O$ in H4 horizons (Fig. 5F). The strong correlation is driven entirely by data from four fossil horizons, plotted as colored squares in Fig. 5E and labeled with arrows in Fig. 4B. The trend is not fossil-specific, as data from brachiopods, crinoids and corals are present in the array. The strong correlation is the result mainly of negative $\Delta^{13}C-\Delta^{18}O$ values, rather than samples positive in both $\Delta^{13}C$ and $\Delta^{18}O$ (Fig. 5E). In shallow-water carbonates, the presence of covarying carbon and oxygen isotopic composition frequently is interpreted as evidence of alteration by meteoric fluids (Allan and Matthews, 1982). Sourced from ^{18}O-depleted rainwater, these fluids often are CO_2-rich due to organic matter degradation in soil profiles; thus, these fluids can create covarying $\delta^{13}C_{carb}-\delta^{18}O_{carb}$ arrays in recrystallized carbonate as they mix with marine waters heavier in both $\delta^{13}C_{carb}$ and $\delta^{18}O_{carb}$ (Allan and Matthews, 1982). This process exerts significant control over $\delta^{13}C_{carb}$ values in Plio-Pleistocene carbonates from the Great Bahama Bank (Melim et al., 2001; Swart and Eberli, 2005), where negative shifts in $\delta^{13}C_{carb}$ are driven by ice-age related sea level falls, subaerial exposure of carbonate banks and
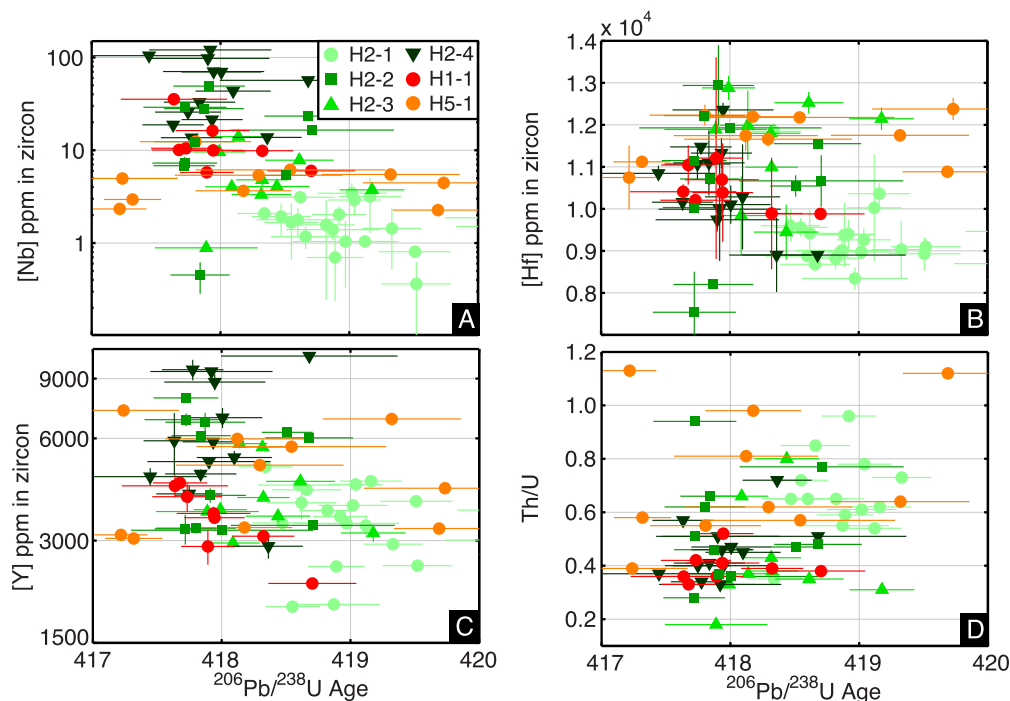
Fig. 7. A selection of results from TIMS-TEA (see section 3.3), with Nb (A), Hf (B) and Y (C) concentrations in zircon plotted against $^{206}Pb/^{238}U$ age. Th/U versus age is displayed in subplot D, although this geochemical parameter was determined via ID-TIMS (see item *(b)* in Table S4).

Table 1
Interpreted depositional ages of Helderberg ashes.

Sample	Height[a]	Formation	$^{206}Pb/^{238}U$ age (Ma)	2σ Error (X/Y/Z)[b]	Method[c]
H2-1	9.0	Kalkberg	418.42	0.21/0.27/0.53	MC
H2-2	12.5	Kalkberg	417.85	0.23/0.29/0.54	MC
H2-3	15.1	Kalkberg	417.73	0.22/0.28/0.53	MC
H2-4	18.4	Kalkberg	417.56	0.20/0.26/0.51	MC
H1-1	44.1	Kalkberg	417.68	0.21/0.27/0.52	YZ
H5-1	84.9	Corriganville	417.22	0.21/0.23/0.50	YZ

[a] In meters; relative to base of measured section (see Fig. 2 caption).
[b] X = internal uncertainty/X + tracer calibration uncertainty/Y + ^{238}U decay constant uncertainty.
[c] MC = Monte Carlo method; YZ = youngest closed-system zircon.

consequent infiltration of coastal pore fluids. This style of diagenesis may have become more common after the late Silurian, given the rise of a terrestrial biosphere (Raven and Edwards, 2001; Gensel, 2008) to serve as biomass in soil profiles.

If a similar process is active in H1, it is happening on a much smaller scale. In meteorically altered bank-top sediments from The Bahamas, the diagenetic front is >100 m thick, resulting in pervasive, fabric-destructive recrystallization and $\delta^{13}C$ offsets of up to 10‰ (Melim et al., 2001). By contrast, observations of covarying fossil $\delta^{13}C$–$\delta^{18}O$ arrays are limited to four horizons from a single stratigraphic section and result in $\delta^{13}C$ offsets of 0.5–1‰ (Fig. 5E). Furthermore, no correlation is observed between $\delta^{13}C_{carb}$ and $\delta^{18}O_{carb}$ in the full Helderberg chemostratigraphic dataset (Figs. 4B, C and S2). Thus, while recrystallization by a $\delta^{13}C$- and $\delta^{18}O$-depleted fluid may explain certain observations in the H1 dataset (*i.e.,* greater variability in fossil $\delta^{13}C$ as compared to H4; instances of covarying $\delta^{13}C$–$\delta^{18}O$ values), it appears to be a local, perhaps permeability-controlled process, affecting certain portions of the stratigraphic record from the more restricted western portion of the Appalachian basin (Rickard, 1962) and resulting in $\delta^{13}C$ offsets of < 1‰.

The results of these fossil-micrite comparisons in the Helderberg Gp. are in broad agreement with similar studies (Samtleben et al., 2001; Batt et al., 2007; Cramer et al., 2010; Brand et al., 2012). These studies focused on brachiopods, and all note generally positive $\Delta^{18}O$ values, ranging between 0.5 and 5‰, similar to observations from the Helderberg Gp. (especially section H4; Fig. 5D). Collectively, these observations suggest less $\delta^{18}O$ resetting to lower values in shell carbonate during diagenesis as compared to coeval micrite. $\Delta^{13}C$ results, however, are more variable, with some indicating zero mean offset (Samtleben et al., 2001; Cramer et al., 2010) and others showing positive mean $\Delta^{13}C$ values of up to 2‰ (Brand et al., 2012). One study (Batt et al., 2007) demonstrated both positive and negative $\Delta^{13}C$ values with considerable variability (up to 7‰), with values depending strongly upon taxon and shell ultrastructure. Thus, fossil-micrite isotopic comparisons must be treated on a case-by-case basis, with the results likely controlled by primary mineralogy of both fossil and micrite (aragonite vs. calcite), shell type, and the burial and diagenetic history of the studied strata. This range of $\Delta^{13}C$ observations highlights the utility of making fossil-micrite comparisons in studies that seek to interpret stratigraphic changes in $\delta^{13}C$ of carbonate rock.

5.2. Implications of Helderberg chemostratigraphic correlations

In the lower Helderberg Gp. of New York and West Virginia, a positive $\delta^{13}C_{carb}$ excursion is recorded consistently across the Ap-
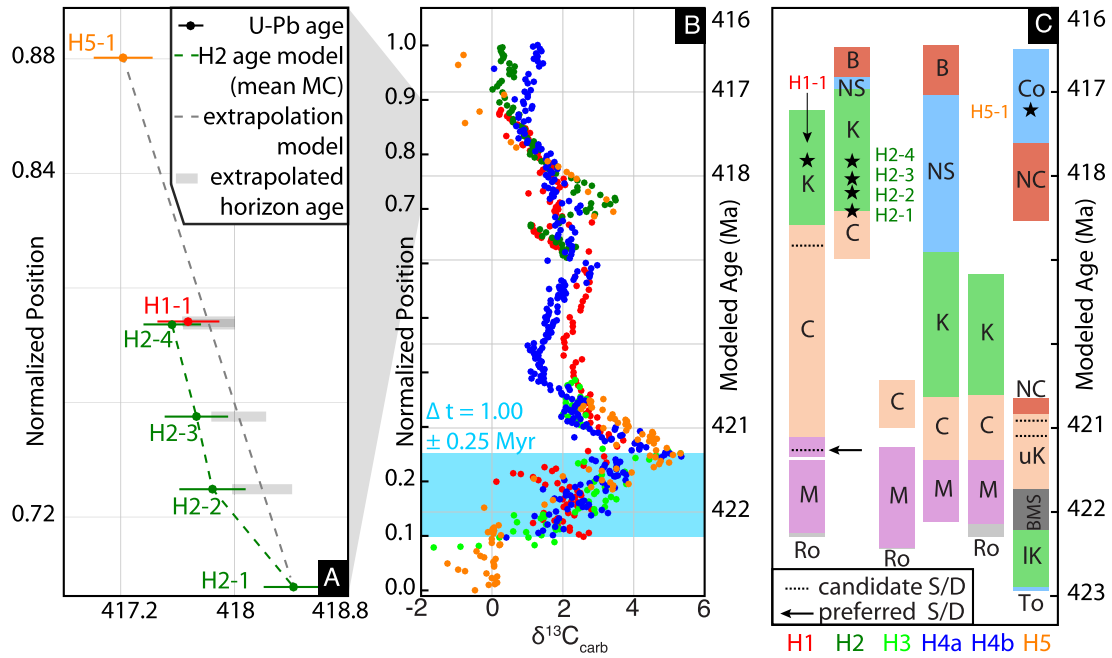
Fig. 8. (A) Normalized positions of dated ash horizons in the Helderberg Gp. chemostratigraphic composite (Fig. 4) plotted against their interpreted depositional age (Fig. 6 and Table 1). The dashed green line shows the age model for portions of section H2 bound by ashes H2-1 to H2-4 (mean value of dark gray Monte Carlo paths in Fig. 6). For all other portions of the composite, the dashed grey line is the extrapolation age model used to develop a $\delta^{13}C_{carb}$ time series (B) and the resulting chronostratigraphy (C) for formations of the Helderberg Gp by the chemostratigraphic correlations presented in Fig. 4. (For interpretation of the references to color in this figure legend, the reader is referred to the web version of this article.)

palachian foreland basin, with values reaching $+5\permil$ (Figs. 2 and 4B). The agreement in measured $\delta^{13}C_{carb}$ values between sections, the congruence between micrite and fossil-phase $\delta^{13}C_{carb}$ measurements (Figs. 4B and 5), and the lack of covariation between $\delta^{13}C_{carb}$ and $\delta^{18}O_{carb}$ (Figs. 4C and S2) suggests that the excursion reflects changes in $\delta^{13}C_{DIC}$, observed at least on the basin-scale.

The composite chemostratigraphy presented in Fig. 4 has two important implications for the Helderberg Gp. Firstly, the composite implies that Helderberg formations are time-transgressive in New York, with the Kalkberg/New Scotland fms. in eastern sections coeval with the Coeymans Fm. in more western sections (Fig. 4A). This result agrees with the oldest stratigraphic model for the Helderberg Gp., which argued that its formations are diachronous across the basin, with formation boundaries younging from the deeper, siltier east (Albany region) towards the more restricted west (Rickard, 1962; Laporte, 1969). This model has since been challenged by claims that Helderberg formation boundaries are isochronous across the basin (Anderson et al., 1984; Demicco and Smith, 2009). These models can be compared directly with our chemostratigraphic dataset from five localities across New York state. Under a correlation scheme where formation boundaries are forced to be isochronous across the state (Fig. S3A, B), the result is visually a much worse fit in $\delta^{13}C_{carb}$ when compared to the diachronous stratigraphic model (Figs. 4A and S3C, D). Thus, if $\delta^{13}C_{carb}$ changes are synchronous across the basin, it lends general support to the diachronous lithofacies model of Rickard (1962) and Laporte (1969), especially for middle portions of Helderberg stratigraphy (*i.e.*, above the base of the Coeymans). Chemostratigraphic correlations suggest that the Rondout and Manlius fms. are broadly synchronous across the basin (also suggested by recent sedimentologic investigations; Demicco and Smith, 2009).

Secondly, the composite makes specific predictions for the correlation of ash-fall horizons across the basin; namely, H2-4 is predicted to be equivalent to H1-1, and H5-1 is the stratigraphically highest ash (Fig. 4B). These relationships are allowable by our geochronologic dataset (Fig. 6), which permits time equivalence

between H2-4 and H1-1 (depositional ages of 417.56 ± 0.20 Ma and 417.68 ± 0.21 Ma, respectively; Table 1) and shows that H5-1 is the youngest ash horizon (417.22 ± 0.22 Ma). To our knowledge, this study is the first in which an intra-basinal chemostratigraphic correlation model has been corroborated by U–Pb geochronology.

5.3. An age model for the Helderberg group

Depositional ages of these six Helderberg ashes (Fig. 6) allow for estimation of the age of the Silurian–Devonian boundary in New York state. In New York, all dated ashes come from the Kalkberg Fm., a unit that contains *I. postwoschmidti* conodonts and can therefore be characterized confidently as Devonian in age (Kleffner et al., 2009). Thus, the age of $418.42 \pm 0.21/0.27/0.53$ Ma ($\pm$ analytical/analytical + tracer calibration/analytical + tracer + ^{238}U decay uncertainties; see Table 1) for H2-1 is a strong minimum age for the base of the Devonian System. Sampled at the Coeymans–Kalkberg boundary in section H2 (Fig. 2), this ash is ~10 m below H1-1/H2-4 (Figs. 2 and 4B), colloquially known as 'Rickard's ash' and the lowest Devonian ash with previously published radiometric constraints (Tucker et al., 1998). The age of H2-1 makes it unlikely that the Silurian–Devonian boundary is on the younger side of its currently assigned uncertainty (419.2 ± 3.2 Ma; Becker et al., 2012).

As the six dated ashes sit stratigraphically above all candidate horizons for the Silurian–Devonian boundary in the Helderberg Gp. (Fig. 4B), downward projection of inferred sedimentation rates is required to estimate its age. While recognizing uncertainty in its placement, our preferred candidate is the lower horizon in section H1 (lower dashed black line in Fig. 2; lower dashed red line in Fig. 4B), corresponding to horizon B in Kleffner et al. (2009). This placement in H1 is justified by (*a*) concordance with a maximum in $\delta^{13}C_{carb}$ values, as seen in sections from Klonk, Czech Republic (Buggisch and Mann, 2004) and (*b*) identification of conodonts referable to the *I. woschmidti* group (but not necessarily to *I. woschmidti woschmidti*; Kleffner et al., 2009). In section H2, a

marked change in apparent sedimentation rate is observed, with a relatively slow rate observed between H2-1 and H2-2 and a faster rate between H2-2 and H2-4 (Fig. 8A). This break makes downward extrapolation challenging, with the selected age model exerting a strong control on the projected age of Silurian–Devonian boundary – much stronger, in fact, than the chosen method used to interpret ages of individual ashes (i.e., weighted mean, youngest zircon or Monte Carlo; see Table S2).

A Monte Carlo approach, similar to the methods used to evaluate depositional ages (section 4.3), can be taken for estimating the age and its uncertainty of a stratigraphic horizon below, between or above two dated ash beds. Using the depositional age with its uncertainty, 10^6 normally distributed numbers are created for each of the two nearest ash beds. 10^6 sedimentation rates, using the stratigraphic separation of the ash beds, are calculated from this paired synthetic dataset, each of which is used to project to the desired stratigraphic height. The mean of the resulting distribution is used as the best estimate of the projected age, while the standard deviation of the distribution is used to estimate its uncertainty (light gray bars in Fig. 8A and Table S2). Under this approach, strata that are bound by ash falls have the most well-constrained numeric ages (i.e., the ~10 m of Kalkberg Fm. between H2-1 and H2-4 in section H2). For horizons that are above or below these ashes, or for horizons found in sections other than H2, a correlation scheme and age model for downward/upward extrapolation are required. For the former, the correlation model presented in Fig. 4 is used, thus linking the ashes, candidate horizons for the Silurian–Devonian boundary and $\delta^{13}C_{carb}$ measurements in a single composite framework.

For the latter, if a linear age model constructed from the most stratigraphically distant ashes in a single section (H2) is used as the best approximation of the long-term sedimentation rate of the Helderberg Gp. (i.e., a hypothetical straight line connecting H2-1 and H2-4 in Fig. 8A), the calculated age of the boundary is $422.5 \pm 1.6/1.6/1.9$ Ma. If H5-1 is used as the upper anchor (the dashed grey line connecting H2-1 and H5-1 in Fig. 8A), implied sedimentation rates are faster (15.3 ± 4.0 m/Ma vs. 10.7 ± 4.0 m/Ma, when the model is projected into section H4). This model yields a Silurian–Devonian boundary age of $421.3 \pm 0.9/0.9/1.2$ Ma. Both of these estimates overlap with the current Silurian–Devonian boundary age of 419.2 ± 3.2 Ma, and are allowable given uncertainties on the highest radiometric age constraint from the Silurian system – an ash found in the upper Whitcliffe Fm. of Ludlow, England, near the Ludlow–Priodoli boundary (Tucker and McKerrow, 1995), whose weighted-mean $^{206}Pb/^{238}U$ age was recalculated by Schmitz (2012) to be 420.88 ± 1.04 Ma (analytical + tracer uncertainty). Assessing which age is more accurate is challenging, given both the ongoing debate of the placement of the Silurian–Devonian boundary in New York (Kleffner et al., 2009) and the uncertainties inherent in both the downward extrapolation of any age model and our correlation model for the Helderberg Gp. We prefer the age of $421.3 \pm 0.9/0.9/1.2$ Ma, as it integrates the most information from the composite stratigraphic section (Figs. 4B and 8A), is least affected by hiatuses (as is observed potentially between ashes H2-1 and H2-2) and is in better agreement with the late Silurian age from Tucker and McKerrow (1995). As these estimates depend upon constant sedimentation rates in section H4 (see section 4.1), as well as the correlation model used for the other sections, the development of more radiometric ages, from both the Helderberg Gp. and other Silurian–Devonian sections, will better constrain both the correlation scheme and the numeric age for the Silurian–Devonian boundary. At present, however, this approach is the best that the data allow.

5.4. Implications for the Silurian–Devonian carbon cycle

Using the chemostratigraphic correlations presented in Fig. 4, this same age model can be used to derive a $\delta^{13}C_{carb}$ time series (Fig. 8B) and a chronostratigraphy for the Helderberg Gp. (Fig. 8C). The model estimates the 'peak time duration' of the Klonk Event, here defined as the basal rise from 0 to 5‰ (Figs. 4B and 8B), to be 1.00 ± 0.25 Myr. Observations of similar $\delta^{13}C_{carb}$ positive shifts in Silurian–Devonian boundary sections from Baltica (Buggisch and Mann, 2004) and other localities in Laurentia (Saltzman, 2002; Fig. 1) support the claim that the Klonk Event represents a perturbation to the global carbon cycle. To assess processes which may be driving a global perturbation, we consider carbon isotope mass balance for an ocean-atmosphere box model:

$$\delta^{13}C_{input} = (1 - f_{org}) * \delta^{13}C_{DIC} + f_{org} * (\delta^{13}C_{DIC} - \varepsilon_{org}), \qquad (1)$$

where $\delta^{13}C_{input}$ is the isotopic value of mantle-derived carbon input to the surface environment ($\sim -6‰$), $\delta^{13}C_{DIC}$ is the isotopic value of the oceanic DIC pool, f_{org} is the fraction of the total carbon burial flux that is organic matter, and ε_{org} is the isotopic fractionation between DIC and organic matter, with a long-term average value of $\sim 30‰$ (Hayes et al., 1999). Under steady-state conditions, where the size of the DIC reservoir (M_c) is not changing and the total carbon burial flux (F_b) equals the mass flux of carbon input (F_{in}), a simple way to cause positive excursions in $\delta^{13}C_{DIC}$ is by increasing f_{org} (Kump et al., 1999), with DIC increasing to a new isotopic value in a time span governed by the residence time of carbon in ocean–atmosphere system (currently ~ 0.1 Ma; Holser et al., 1988). Adapting equation 2 from Kump and Arthur (1999), the rate of isotopic change in response to a forcing from f_{org} is expressed as:

$$\frac{d\delta^{13}C_{DIC}}{dt} = \frac{F_{in}}{M_c} * \Big(\delta^{13}C_{input} - (1 - f_{org}) * \delta^{13}C_{DIC}$$
$$+ f_{org} * (\delta^{13}C_{DIC} - \varepsilon_{org}) \Big). \qquad (2)$$

To determine whether such a model can explain the Klonk Event, we numerically solve equation (2) for $\delta^{13}C_{DIC}$ following a step increase in f_{org} from 0.20 to 0.37. For a range of values of F_{in} and M_c, synthetic time-series of evolving $\delta^{13}C_{DIC}$ are produced (Fig. 9A). The DIC 'response time' is defined as the amount of time required for $\delta^{13}C_{DIC}$ to rise to 4.95‰ following the perturbation (colored circles in Fig. 9A). Fig. 9B is a plot of these response times as a function of DIC reservoir size, contoured for values of F_{in} as multiples of the modern value. Given the estimated peak time duration of 1.0 ± 0.25 Ma, modern fluxes of carbon can explain the Klonk Event, so long as DIC remained below $\sim 2\times$ modern levels. As an upper limit consideration, if models that contend Devonian DIC was $\sim 4\times$ modern levels (Berner and Kothavala, 2001) are correct, carbon fluxes must have been 2–$3\times$ the modern value in order for the excursion to be explained in a steady-state framework (Fig. 9B). If an alternative age model is used to constrain the excursion (i.e., using H2-1 and H2-4 as the anchors in Fig. 8A), the duration is longer (1.4 ± 0.5 Ma), and allows for a steady-state solution under the modern flux value and higher DIC levels ($\sim 3\times$ modern levels). While it is unlikely that the forcing that drove the Klonk Event was truly a step function, this approach produces response times that are as fast as possible for a given reservoir size and flux, and thus should be viewed as producing end-member constraints. In other words, if Devonian DIC = 6 mM, then the Devonian carbon input flux needed to be at least $\sim 2\times$ the modern value (Fig. 9), or more if the change in f_{org} was more gradual.

The unique biotic and tectonic circumstances of the Silurian–Devonian transition make an increase in f_{org} a plausible driver. The radiation of land plants (Gensel, 2008), coupled with the
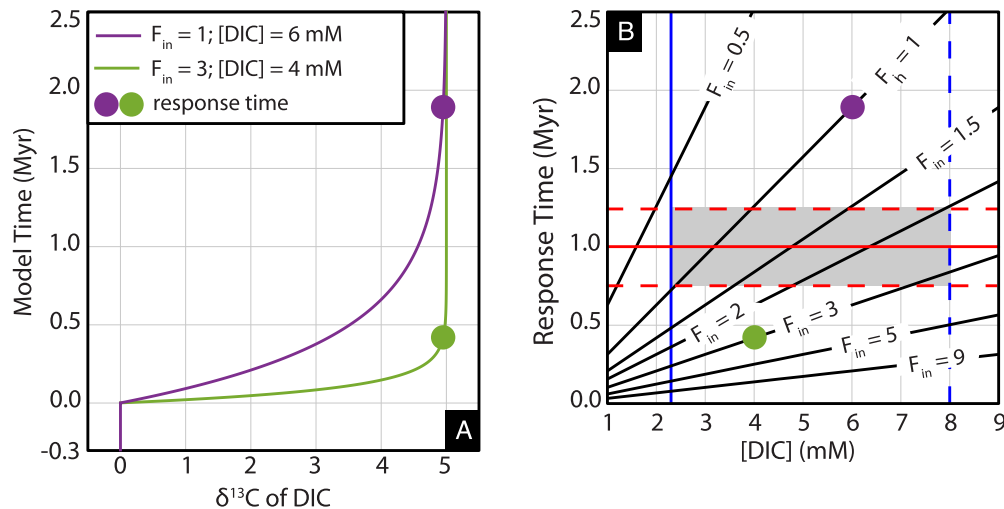
Fig. 9. (A) Solutions to equation (2) after a step change in f_{org} from 0.20 to 0.37 for different values of DIC reservoir size and carbon input flux (F_{in}; expressed as multiples of the modern flux). The response time, here defined as the amount of time for $\delta^{13}C_{DIC}$ to rise to 4.95‰, is labeled with colored circles. (B) Response times can be calculated for a range of parameter values; here they are plotted as a function of [DIC], contoured for values of F_{in} as multiples of the modern value. The present concentration of DIC is marked with a solid blue line. As an upper limit consideration, we plot the model prediction of Berner and Kothavala (2001) that Early Devonian DIC was ∼4× modern levels (dashed blue line). Horizontal solid and dashed red lines depict the estimated peak time duration with uncertainties, respectively, for the Silurian–Devonian $\delta^{13}C_{carb}$ excursion derived from the U–Pb age constraints from the H2-1 and H5-1 ashes (dashed grey line in Fig. 8A). Thus, the shaded grey region is the phase space of allowed model values (duration, DIC levels and carbon flux) in which the excursion could proceed under steady-state conditions. (For interpretation of the references to color in this figure legend, the reader is referred to the web version of this article.)

diachronous closure of the Rheic ocean and global Caledonian orogeny (Nance et al., 2010), created conditions amenable to enhanced burial of organic matter, with the development of fast-sedimenting clastic wedges along the paleotropical margins of Laurentia and Baltica (Malkowski and Racki, 2009). Reasons why these conditions resulted in a transient excursion rather than a longer-lived state change to higher values of f_{org} may lie in feedbacks between increased surface oxygenation and increased organic carbon remineralization efficiency.

Alternatively, sedimentary environments well-suited to organic carbon burial also are ideal for the precipitation of authigenic carbonate in the sediment column (Aller et al., 1996), which has recently been proposed as an important third sink when considering redox implications of $\delta^{13}C$ values and time series (Schrag et al., 2013). As this sink often is negative isotopically compared to marine carbonate, increasing the fraction of F_b that is authigenic carbonate in a steady state framework also can cause rises in $\delta^{13}C_{DIC}$, without the same implications of an increased O_2 flux to the surface environment. Tests for discriminating which driver is more important include (a) documentation of an increase in authigenic carbonate phases hosted in Silurian–Devonian siliciclastic successions and (b) independent assessment of the redox state across the Silurian–Devonian boundary, as an increase in the oxidative power of the surface environment would be consistent with an increase in the burial fraction of organic matter.

6. Conclusions

A 5‰ positive shift in $\delta^{13}C_{carb}$ is recorded in shallow-water carbonates of the Helderberg Group of North America. The chemostratigraphic dataset is calibrated by U–Pb ages on six intercalated ash falls, which corroborates the developed intrabasinal correlation scheme, as well as allowing estimation of the Klonk Event duration and age of the Silurian–Devonian boundary. We estimate the Silurian–Devonian boundary age in New York to be 421.3 ± 1.2 Ma (2σ; including decay constant uncertainties) in New York, and calculate the peak time duration of the Silurian–Devonian boundary $\delta^{13}C_{carb}$ excursion to be 1.00 ± 0.25 Myr. Under these constraints, a steady-state perturbation to the global carbon cycle can explain the observed excursion with modern carbon fluxes, as long as DIC

concentration in the Devonian ocean remained below ∼2× the modern value, although discriminating between increased organic carbon burial or authigenic carbon burial as the more likely driver for the excursion requires further investigation of the redox state of the surface environment across the Silurian–Devonian boundary.

Appendix A. Supplementary material

Supplementary material related to this article can be found online at http://dx.doi.org/10.1016/j.epsl.2015.11.044.

References

Allan, J., Matthews, R., 1982. Isotope signatures associated with early meteoric diagenesis. Sedimentology 29, 797–817.

Aller, R.C., Blair, N.E., Xia, Q., Rude, P.D., 1996. Remineralization rates, recycling, and storage of carbon in Amazon shelf sediments. Cont. Shelf Res. 16, 753–786.

Alroy, J., et al., 2008. Phanerozoic trends in the global diversity of marine invertebrates. Science 321, 97–100.

Anderson, E., Goodwin, P., Sobieski, T., 1984. Episodic accumulation and the origin of formation boundaries in the Helderberg Group of New York State. Geology 12, 120–123.

Batt, L.S., Montañez, I.P., Isaacson, P., Pope, M.C., Butts, S.H., Abplanalp, J., 2007. Multi-carbonate component reconstruction of mid-Carboniferous (Chesterian) seawater $\delta^{13}C$. Palaeogeogr. Palaeoclimatol. Palaeoecol. 256, 298–318.

Becker, R., Gradstein, F., Hammer, O., 2012. The Devonian period. In: Gradstein, F., Ogg, J., Schmitz, M., Ogg, G. (Eds.), The Geologic Time Scale, vol. 2. Elsevier, Amsterdam, pp. 559–601.

Berner, R.A., Kothavala, Z., 2001. GEOCARB III: a revised model of atmospheric CO_2 over Phanerozoic time. Am. J. Sci. 301, 182–204.

Bowring, J.F., McLean, N.M., Bowring, S.A., 2011. Engineering cyber infrastructure for U–Pb geochronology: Tripoli and U–Pb_Redux. Geochem. Geophys. Geosyst. 12.

Brand, U., Jiang, G., Azmy, K., Bishop, J., Montañez, I.P., 2012. Diagenetic evaluation of a Pennsylvanian carbonate succession (Bird Spring Formation, Arrow Canyon, Nevada, USA) – 1: Brachiopod and whole rock comparison. Chem. Geol. 308, 26–39.

Buggisch, W., Mann, U., 2004. Carbon isotope stratigraphy of Lochkovian to Eifelian limestones from the Devonian of central and southern Europe. Int. J. Earth Sci. 93, 521–541.

Carls, P., Slavík, L., Valenzuela-Ríos, J.I., 2007. Revisions of conodont biostratigraphy across the Silurian–Devonian boundary. Bull. Geosci. 82, 145–164.

Clarke, J.M., Schuchert, C., 1899. The nomenclature of the New York series of geological formations. Science, 874–878.

Condon, D., Schoene, B., McLean, N., Bowring, S., Parrish, R., 2015. Metrology and traceability of U–Pb isotope dilution geochronology (EARTHTIME Tracer Calibration Part I). Geochim. Cosmochim. Acta 164, 464–480.

Cramer, B.D., Loydell, D.K., Samtleben, C., Munnecke, A., Kaljo, D., Männik, P., Martma, T., Jeppsson, L., Kleffner, M.A., Barrick, J.E., et al., 2010. Testing the limits of Paleozoic chronostratigraphic correlation via high-resolution (<500 ky) integrated conodont, graptolite, and carbon isotope ($\delta^{13}C_{carb}$) biochemostratigraphy across the Llandovery–Wenlock (Silurian) boundary: is a unified Phanerozoic time scale achievable? Geol. Soc. Am. Bull. 122, 1700–1716.

Demicco, R., Smith, J., 2009. Sedimentologic observation and stratigraphic interpretation of the Lower Devonian (Lochkovian) Manlius Formation along the Mohawk River Valley in upstate New York. J. Geol. 117, 543–551.

Denkler, K., Harris, A., 1988. Conodont-based determination of the Silurian-Devonian boundary in the Valley and Ridge Province, northern and central Appalachians. U.S. Geol. Surv. Bull. 1837, B1–B13.

Dorobek, S., 1987. Petrography, geochemistry, and origin of burial diagenetic facies, Siluro–Devonian Helderberg Group (carbonate rocks), central Appalachians. Am. Assoc. Pet. Geol. Bull. 71.

Gensel, P.G., 2008. The earliest land plants. Annu. Rev. Ecol. Evol. Syst. 39, 459–477.

Guex, J., Schoene, B., Bartolini, A., Spangenberg, J., Schaltegger, U., O'Dogherty, L., Taylor, D., Bucher, H., Atudorei, V., 2012. Geochronological constraints on post-extinction recovery of the ammonoids and carbon cycle perturbations during the Early Jurassic. Palaeogeogr. Palaeoclimatol. Palaeoecol. 346, 1–11.

Hanson, B., 1995. A geochemical study of rhyolitic melt inclusions in igneous phenocrysts from lower Devonian bentonites. Ph.D. thesis. State University of New York, Albany.

Hayes, J., Strauss, H., Kaufman, A., 1999. The abundance of ^{13}C in marine organic matter and isotopic fractionation in the global biogeochemical cycle of carbon during the past 800 Ma. Chem. Geol. 161, 103–125.

Holser, W., Schidlowski, M., Mackenzie, F., Maynard, J., 1988. Geochemical cycles of carbon and sulfur. In: Gregory, C., Garrels, R., Mackenzie, F., Maynard, J. (Eds.), Chemical Cycles in the Evolution of the Earth. Wiley, John & Sons, pp. 105–173.

Kleffner, M.A., Barrick, J.E., Ebert, J.R., Matteson, D., Karlsson, H., 2009. Conodont biostratigraphy, $\delta^{13}C$ chemostratigraphy, and recognition of Silurian/Devonian boundary in the Cherry Valley, New York region of the Appalachian Basin. Palaeontogr. Am. 62, 57–73.

Kump, L., Arthur, M., 1999. Interpreting carbon-isotope excursions: carbonates and organic matter. Chem. Geol. 161, 181–198.

Kump, L., Arthur, M., Patzkowsky, M., Gibbs, M., Pinkus, D., Sheehan, P., 1999. A weathering hypothesis for glaciation at high atmospheric pCO_2 during the Late Ordovician. Palaeogeogr. Palaeoclimatol. Palaeoecol. 152, 173–187.

Laporte, L., 1969. Recognition of a transgressive carbonate sequence within an epeiric sea: Helderberg Group (Lower Devonian) of New York State: Depositional Environments in Carbonate Rocks. In: Society of Economic Paleontologists and Mineralogists Special Publication, vol. 14, pp. 98–119.

Malkowski, K., Racki, G., 2009. A global biogeochemical perturbation across the Silurian-Devonian boundary: ocean–continent–biosphere feedbacks. Palaeogeogr. Palaeoclimatol. Palaeoecol. 276, 244–254.

Maloof, A.C., Ramezani, J., Bowring, S.A., Fike, D.A., Porter, S.M., Mazouad, M., 2010. Constraints on early Cambrian carbon cycling from the duration of the Nemakit–

Daldynian–Tommotian boundary $\delta^{13}C$ shift, Morocco. Geology 38, 623–626.

Mattinson, J., 2005. Zircon U–Pb chemical abrasion ("CA-TIMS") method: combined annealing and multi-step partial dissolution analysis for improved precision and accuracy of zircon ages. Chem. Geol. 220, 47–66.

McLean, N.M., Bowring, J.F., Bowring, S.A., 2011. An algorithm for U–Pb isotope dilution data reduction and uncertainty propagation. Geochem. Geophys. Geosyst. 12.

McLean, N.M., Condon, D.J., Schoene, B., Bowring, S.A., 2015. Evaluating uncertainties in the calibration of isotopic reference materials and multi-element isotopic tracers (EARTHTIME Tracer Calibration Part II). Geochim. Cosmochim. Acta 164, 481–501.

Melim, L.A., Swart, P.K., Maliva, R.G., 2001. Meteoric and marine-burial diagenesis in the subsurface of Great Bahama Bank. Spec. Publ.-SEPM 70, 137–162.

Meyers, S.R., Siewert, S.E., Singer, B.S., Sageman, B.B., Condon, D.J., Obradovich, J.D., Jicha, B.R., Sawyer, D.A., 2012. Intercalibration of radioisotopic and astrochronologic time scales for the Cenomanian–Turonian boundary interval, Western Interior Basin, USA. Geology 40, 7–10.

Nance, R.D., Gutiérrez-Alonso, G., Keppie, J.D., Linnemann, U., Murphy, J.B., Quesada, C., Strachan, R.A., Woodcock, N.H., 2010. Evolution of the Rheic Ocean. Gondwana Res. 17, 194–222.

Raven, J., Edwards, D., 2001. Roots: evolutionary origins and biogeochemical significance. J. Exp. Bot. 52, 381–401.

Rickard, L., 1962. Late Cayugan (Upper Silurian) and Helderbergian (Lower Devonian) stratrigraphy in New York: 386. University of the State of New York, State Education Dept.

Saltzman, M., 2002. Carbon isotope ($\delta^{13}C$) stratigraphy across the Silurian-Devonian transition in North America: evidence for a perturbation of the global carbon cycle. Palaeogeogr. Palaeoclimatol. Palaeoecol. 187, 83–100.

Saltzman, M., Young, S., 2005. Long-lived glaciation in the Late Ordovician? Isotopic and sequence-stratigraphic evidence from western Laurentia. Geology 33, 109–112.

Samtleben, C., Munnecke, A., Bickert, T., Pätzold, J., 2001. Shell succession, assemblage and species dependent effects on the C/O-isotopic composition of brachiopods – examples from the Silurian of Gotland. Chem. Geol. 175, 61–107.

Schmitz, M., 2012. The radiometric ages used in the GTS2012. In: Gradstein, F., Ogg, J., Schmitz, M., Ogg, G. (Eds.), The Geologic Time Scale, vol. 2. Elsevier, Amsterdam, pp. 1045–1124.

Schoene, B., Crowley, J., Condon, D., Schmitz, M., Bowring, S., 2006. Reassessing the uranium decay constants for geochronology using ID-TIMS U–Pb data. Geochim. Cosmochim. Acta 70, 426–445.

Schoene, B., Guex, J., Bartolini, A., Schaltegger, U., Blackburn, T.J., 2010a. Correlating the end-Triassic mass extinction and flood basalt volcanism at the 100 ka level. Geology 38, 387–390.

Schoene, B., Latkoczy, C., Schaltegger, U., Günther, D., 2010b. A new method integrating high-precision U–Pb geochronology with zircon trace element analysis (U–Pb TIMS-TEA). Geochim. Cosmochim. Acta 74, 7144–7159.

Schrag, D.P., Higgins, J.A., Macdonald, F.A., Johnston, D.T., 2013. Authigenic carbonate and the history of the global carbon cycle. Science 339, 540–543.

Swart, P., Eberli, G., 2005. The nature of the $\delta^{13}C$ of periplatform sediments: implications for stratigraphy and the global carbon cycle. Sediment. Geol. 175, 115–129.

Tucker, R., Bradley, D., Ver Straeten, C., Harris, A., Ebert, J., McCutcheon, S., 1998. New U–Pb zircon ages and the duration and division of Devonian time. Earth Planet. Sci. Lett. 158, 175–186.

Tucker, R., McKerrow, W., 1995. Early Paleozoic chronology: a review in light of new U–Pb zircon ages from Newfoundland and Britain. Can. J. Earth Sci. 32, 368–379.

Ver Straeten, C., 2004. K-bentonites, volcanic ash preservation, and implications for Early to Middle Devonian volcanism in the Acadian orogen, eastern North America. Geol. Soc. Am. Bull. 116, 474–489.

Wright, N., Zahirovic, S., Müller, R., Seton, M., 2013. Towards community-driven paleogeographic reconstructions: integrating open-access paleogeographic and paleobiology data with plate tectonics. Biogeosciences 10, 1529–1541.